Study of the photodetachment of C^- and F^- by many-body perturbation theory*

Takeshi Ishihara
Institute for Pure and Applied Physical Sciences, University of California at San Diego, La Jolla, California 92037

and

Theodore C. Foster
Department of Physics, California Polytechnic State University, San Luis Obispo, California 93401

(Received 18 October 1973)

Photodetachment cross sections of C^- and F^- are calculated by means of the many-body perturbation theory with multiple basis sets. The V^{N-1} basis set is defined to include the intrachannel interaction. The V^{N-2} basis set is introduced to describe the correlation in the Hartree-Fock ground states of negative ions. The lowest-order cross sections agree very well with experiment. The first-order corrections are calculated in the case of F^-, and a large cancellation is found between the initial-state correlation and the final-state interchannel interactions. The importance of the use of the consistent energy relations in the lower-order calculations is pointed out.

I. INTRODUCTION

In the past decade, the photodetachment of negative ions has been investigated, experimentally and theoretically, by many authors primarily because of the astrophysical interest. The effect of core polarization, which is important in the threshold behavior,[1] has been taken into account in most of the theoretical calculations. However, the core-polarization effect alone does not explain the shape of the cross section satisfactorily over the energy range of measurements.[2,3]

Recently, the many-body perturbation theory (MBPT) has been applied to the photoionization of neutral atoms,[4,5] taking into account the correlation effects. It has also been applied[6] to the photodetachment of O^-. In this method, one can give a simple physical interpretation to each contributing term. We present, in this paper, a calculation of the photodetachment cross section of C^- and F^- using the MBPT with multiple basis sets.[7]

On defining a basis set of MBPT expansion for atomic problems, we usually use the Hartree-Fock (HF) orbitals for the occupied states. This may be a reasonable choice for the photodetachment of negative ions, since it is essentially a single-particle process. There is a freedom for excited orbitals to form a complete set together with the HF ground-state orbitals, and we construct them from the HF (V^N) complete set to eliminate certain higher-order diagrams. A description of our method for the photoionization problems was given elsewhere.[5] In the following, we shall neglect the contribution from the inner-shell electrons. In terms of HF (V^N) complete sets, the following correction terms appear in the first order. (i) Particle-hole interaction in the final states. The diagonal interaction, including higher-order ladders, transforms the V^N complete set to the more physical V^{N-1} set.[8] The nondiagonal interactions include inter- and intrachannel interactions described by Fano and Cooper.[9] (ii) Virtual two-particle excitation in the initial state. The effects of polarization and rearrangement of the core, including the correction to the HF values of electron affinities, appear as the second-order processes.

In Sec. II, we define a V^{N-1} complete set which includes the intrachannel interaction. Also, the calculated lowest-order (single-particle model) cross sections of C^- and F^- are compared with experimental measurements. We calculate, in Sec. III, the cross section of F^- with the first-order correction in both initial and final states. Discussions on the second-order processes are given in Sec. IV. We use atomic units throughout this paper.

II. LOWEST-ORDER CROSS SECTIONS OF PHOTODETACHMENT OF C^- AND F^-

A. V^{N-1} complete set

As we have mentioned in Sec. I, we take HF orbitals calculated by Clementi[10] as the ground-state orbitals. The spin-orbit interaction is neglected. The excited-state orbitals are defined as

$$\phi_{klm}(\vec{r}) = \frac{P_{kl}(r)}{r} Y_{lm}(\hat{r}), \tag{1}$$

where $P_{kl}(r)$ satisfies the following equation

$$\left[-\frac{1}{2}\left(\frac{d^2}{dr^2}-\frac{l(l+1)}{r^2}\right)+V_l^{\mathrm{HF}}+U_l\right]P_{kl}(r)=\epsilon_k P_{kl}(r), \tag{2}$$

with the asymptotic form

$$P_{kl}(r)\sim \sin(kr-\tfrac{1}{2}l\pi+\delta_l), \tag{3}$$

where $\epsilon_k=\frac{1}{2}k^2$, V_l^{HF} is the HF (V^N) potential, and U_l can be chosen freely[7] and is defined below to include the intrachannel interaction.

Our choice of U_l is given diagrammatically in Fig. 1, and is written explicitly for s and d states as, in the usual notation,

$$U_s P_{ks}(r)=-\frac{Y_0(2p,2p)}{r}P_{ks}(r)+C_s\frac{Y_1(2p,ks)}{r}P_{2p}(r)+\alpha_{1s}P_{1s}(r)+\alpha_{2s}P_{2s}(r), \tag{4}$$

$$U_d P_{kd}(r)=-\frac{Y_0(2p,2p)}{r}P_{kd}(r)+C_d\frac{Y_1(2p,kd)}{r}P_{2p}(r), \tag{5}$$

where α_{1s} and α_{2s} are given by

$$\alpha_{ns}=\langle ns,2p\,|\,v_0\,|\,ks,2p\rangle-C_s\langle ns,2p\,|\,v_0\,|\,2p,ks\rangle. \tag{6}$$

$$C_s=\begin{cases}\frac{1}{3}\ (\mathrm{C}^-),\\ \frac{2}{3}\ (\mathrm{F}^-),\end{cases}$$

and

$$C_d=\begin{cases}\frac{2}{3}\ (\mathrm{C}^-),\\ \frac{4}{3}\ (\mathrm{F}^-).\end{cases}$$

Quadrupole and octopole interactions have been neglected in Eq. (5).

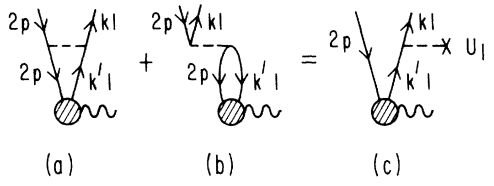

FIG. 1. Diagrammatic definition of U_l. Summation over all possible l_z and spin states in the intermediate state is intended in diagram (b): (a) is a direct particle-hole interaction which removes the Coulomb tail of V_l^{HF}; (b) is an intrachannel interaction which gives rise to a short-range repulsion.

In Eqs. (4) and (5), the first term on the right-hand side refers to diagram (a) of Fig. 1 and removes the Coulomb tail of $V_l^{\mathrm{HF}}(V^N-V^{N-1})$, while the second term refers to diagram (b) and represents the intrachannel interactions. The last two terms of Eq. (4) orthogonalize the excited s state P_{ks} with P_{1s} and P_{2s}. With this complete set, the intrachannel interactions are eliminated in our perturbation expansion of the transition matrix.

B. Cross sections

Photodetachment cross sections (dipole velocity formula) for C^- and F^- in the lowest order are given by[11]

$$\sigma^v=(5.1355\times10^{-18}\ \mathrm{cm}^2)\frac{1}{\omega k}\times\{|\langle ks|\,D\,|2p\rangle|^2\,C_s+|\langle kd|\,D\,|2p\rangle|^2\,C_d\}, \tag{7}$$

where

$$\langle n'l\pm1\,|D|\,nl\rangle=\int_0^\infty dr\,P_{n'l\pm1}(r)\times\left(\frac{d}{dr}\mp\frac{2l+1\pm1}{2r}\right)P_{nl}(r), \tag{8}$$

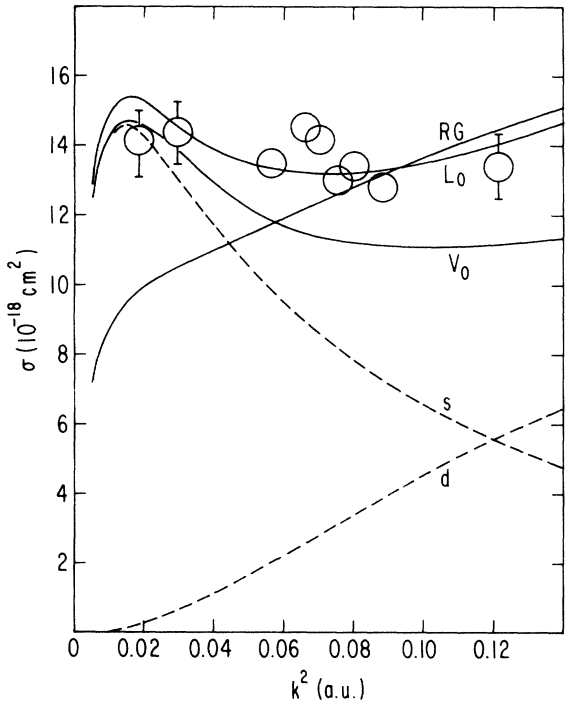

FIG. 2. Photodetachment cross section of C^- in the single-particle approximation. V_0 and L_0 are our velocity and length cross sections, s and d are s- and d-channel contributions to V_0. RG is the calculation of Robinson and Geltman (Ref. 3), experimental results are from Ref. 12.

and the continuum wave functions are normalized as Eq. (3). $\omega = \epsilon_k + \epsilon_i$ is the photon energy with ϵ_i being the electron affinity. In the lowest order, i.e., the single-particle approximation, ϵ_i takes the HF value,[10] $\epsilon_i = -\epsilon_{2p} = 0.07687$ for C^- and 0.18079 for F^-. They are quite different from experimental values,[12,13] $\epsilon_i^{\text{expt}} = 0.04594$ (C^-) and 0.1267 (F^-). The correction to the HF electron affinity will be discussed in Sec. IV.

The dipole-length formula for the lowest-order cross section is given by[11]

$$\sigma^L = (5.1355\times 10^{-18}\ \text{cm}^2)\frac{\omega}{k}\{|\langle ks|r|2p\rangle|^2 C_s + |\langle kd|r|2p\rangle|^2 C_d\}. \quad (9)$$

Equation (9) can be shown to be equivalent to Eq. (7), assuming $\epsilon_i = \epsilon_i^{\text{HF}}$ and

$$\langle kl|(V_i^{\text{HF}} + U_i)r - rV_p^{\text{HF}}|2p\rangle \approx 0. \quad (10)$$

The cross sections calculated by Eqs. (7) and (9) are shown and compared with the experiments[12,14] in Figs. 2 and 3 for C^- and F^-, respectively. The agreement with experiment is very good. The length-velocity difference comes from the neglect of the left-hand side of Eq. (10) in the length formula. In these figures, we plotted the cross sections calculated by Robinson and Geltman[3] for the sake of comparison. They used the single-particle model with the Herman-Skillman potential and the polarization potential. The s- and d-state channel contributions in our cross sections are also shown in these figures.

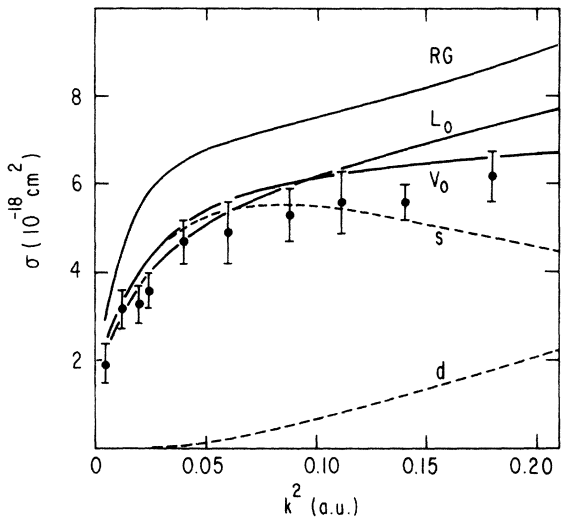

FIG. 3. Photodetachment cross section of F^- in the single-particle approximation. V_0 and L_0 are our velocity and length cross sections, s and d are s- and d-channel contributions to V_0. RG is the calculation of Robinson and Geltman (Ref. 3), experimental results are from Ref. 14.

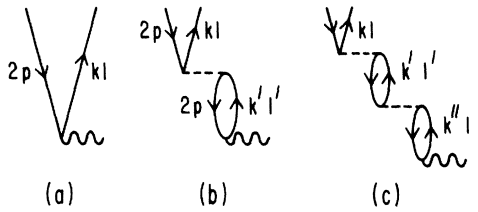

FIG. 4. Final-state correlation: (a) is the lowest-order matrix element, (b) and (c) are the first- and second-order corrections to it through interchannel interaction. $l, l' = 0$ or 2. $l' \neq l$.

III. FIRST-ORDER CORRELATION IN THE PHOTODETACHMENT OF F^-

In the MBPT expansion of the transition matrix in terms of our V^{N-1} basis set, the first-order correction in the final state is the interchannel interaction shown in the diagram (b) of Fig. 4. We neglect the contribution from the inner-shell electrons. The diagram (c) is the second-order correction of this type while the diagram (a) is the zero-order matrix element $\langle kl|D|2p\rangle$. The contribution from the diagram (b) is given by

$$C_{l'}\sum_{k'}\langle kl\,2p|v_1|2pk'l'\rangle \times\frac{1}{\epsilon_k - \epsilon_{k'} + i\eta}\langle k'l'|D|2p\rangle,$$

which should be added to the matrix element $\langle kl|D|2p\rangle$ in Eq. (7) where l and l' are 0 or 2 with $l' \neq l$, and $\eta = +0$.

Diagrams (a) and (b) of Fig. 5 are the correction terms due to the first-order correlation in the initial state. These diagrams include a virtual two-particle excited state and our basis set may

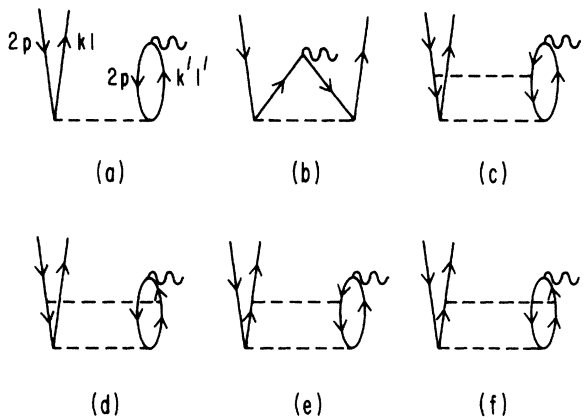

FIG. 5. Initial-state correlation: (a) and (b) are the first-order corrections, (c)–(f) are the related second-order corrections.

not give a good description of it. Reflecting this fact, some related higher-order diagrams become important, namely the diagrams (c)–(f), etc., for the diagram (a), and similar for the exchange diagram (b). The diagram (c) and its ladders can be taken into account by the use of the usual shifted energy denominator[8] in (a).

A particle-hole interaction, Fig. 5(d), and its ladders can be included if we introduce a new complete set $|\tilde{k}l\rangle$, which may be called V^{N-2}, and replace Fig. 5(a) by Fig. 6(a). Where $\tilde{P}_{kl}(r)$ is defined by

$$\left[-\frac{1}{2}\left(\frac{d^2}{dr^2}-\frac{l(l+1)}{r^2}\right)+V_l^{\mathrm{HF}}+U_l+\tilde{U}_l\right]\tilde{P}_{kl}(r)=\tilde{\epsilon}_{kl}\tilde{P}_{kl}(r)\ , \tag{11}$$

with

$$\tilde{U}_l\tilde{P}_{kl}(r)=-\frac{Y_0(2p,2p)}{r}\tilde{P}_{kl}(r)+F_l(r), \tag{12}$$

$F_l(r)$ is to orthogonalize $\tilde{P}_{kl}$ with the ground-state orbitals, and for s and d states,

$$F_l(r)=\begin{cases}P_{1s}(r)\langle 1s2p|v_0|\tilde{k}s2p\rangle+p_{2s}(r)\langle 2s2p|v_0|\tilde{k}s2p\rangle, & l=0\\ 0, & l=2.\end{cases}$$

In the above definition of $\tilde{U}_l$, we have neglected the exchange and quadrupole interactions. The potential in the above Schrödinger equation behaves asymptotically as $(-1/r)$ and, therefore, this V^{N-2} complete set includes bound excited states. Similarly, we can add up Fig. 5(e) and its ladders to give the diagram (c) of Fig. 6. Because of the sharp peak of the overlap integral[7] $\langle kl|\tilde{k}''l\rangle$, the dominant contribution comes from the diagram with $|\tilde{k}''l\rangle$ in continuum states of $k''\approx k$ and $|\tilde{k}'l'\rangle$ in the lowest bound state in which the particle-particle interaction may largely screen the particle-hole interaction taken above in the continuum state $|\tilde{k}''l\rangle$. Thus, Fig. 5(a) together with the important higher-order terms may be given, in a good approximation, by a single diagram, Fig. 6(a). Similarly, we have Fig. 6(b) for the exchange diagram.

The contributions from these diagrams (a) and (b) to be added to the matrix element $\langle kl|D|2p\rangle$ in Eq. (7) are expressed as

$$\sum_{l'=0,2} C_{l'}\langle 2p|D|\tilde{k}'l'\rangle\frac{1}{E_0-\tilde{\epsilon}_{k'l'}-\epsilon_k}\langle kl\tilde{k}'l'|v_1|2p2p\rangle$$

and

$$\sum_{l'=0,2} C(l,l')\langle 2p|D|\tilde{k}'l'\rangle \times\frac{1}{E_0-\tilde{\epsilon}_{k'l'}-\epsilon_k}\langle kl\tilde{k}'l'|v_1|2p2p\rangle,$$

respectively. The angular factors in the latter expression are given by

$$C(l,0)=-\tfrac{1}{3},\ C(0,2)=-\tfrac{2}{3},\ C(2,2)=-\tfrac{1}{15},$$

and

$$E_0=2\epsilon_{2p}-\langle 2p2p|v_0|2p2p\rangle.$$

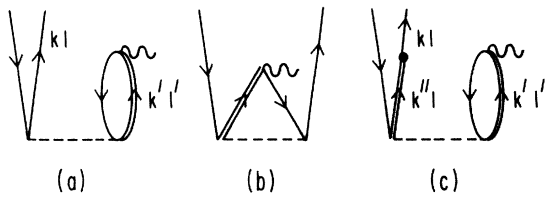

FIG. 6. Initial-state correlation diagrams with multiple basis sets. Double lines stand for the V^{N-2} complete set, defined by Eq. (11). Dot in diagram (c) is the overlap integral $\langle kl|\tilde{k}''l\rangle$ of two complete sets (Ref. 7).

Figure 7 shows the F^- photodetachment cross section of zeroth order (diagram 4-a only), with the first-order final-state correlation (diagrams 4-a and 4-b) and with both initial- and final-state correlations [diagrams 4(a), 4(b), 6(a), and 6(b)]. The second-order final-state correlation of Fig. 4(c) affects the cross section very little (~0.1 $\times 10^{-18}$ cm^2 over our energy range).

IV. DISCUSSION AND CONCLUSIONS

We have shown, in Sec. II, the results of our single-particle-model calculation of the photodetachment cross sections of C^- and F^-. They

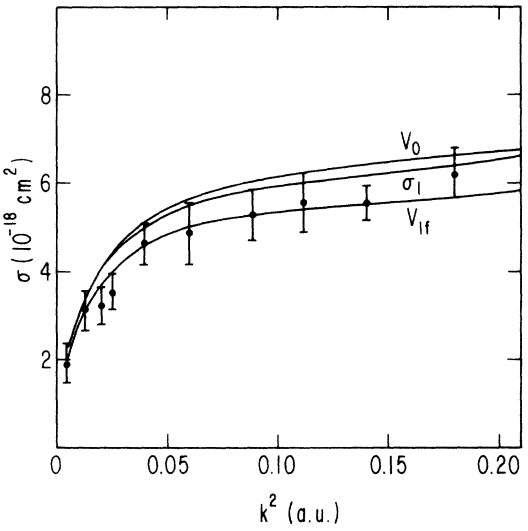

FIG. 7. Cross section of F^- in the first order. The velocity formula is used. V_0 is the lowest-order cross section (diagram 4-a only), V_{1f} with the final-state correlation (sum of diagrams 4-a and 4-b), σ_1 with both initial- and final-state correlation [sum of diagrams 4(a), 4(b), 6(a), and 6(b).

are in very good agreement with experimental measurements. It has also been shown, in Sec. III, that the first-order correlations in the initial and final states largely cancel each other in the case of F^-. The situation perhaps is the same for C^-. The comparison with other single-particle calculations, such as those of Robinson and Geltman, shows the importance of the intrachannel interaction which gives rise to the exchange-type repulsion for the free electron. See the second terms of the right-hand sides of Eqs. (4) and (5).

In our calculation, Hartree-Fock energy of $2p$ orbital has been used as the electron affinity consistently with our single-particle wave functions. This is somewhat uncomfortable because the HF values differ so much from the experimental values of the electron affinity: $\epsilon_i^{expt} = 0.045\,94$ for C^- and 0.1267 for F^-, while $\epsilon_i^{HF} = 0.076\,87$ for C^- and $0.180\,79$ for F^-. The correction terms to change ϵ_i^{HF} to ϵ_i^{expt} in the cross-section formula,

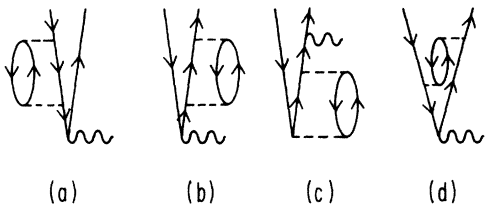

FIG. 8. Typical second-order corrections.

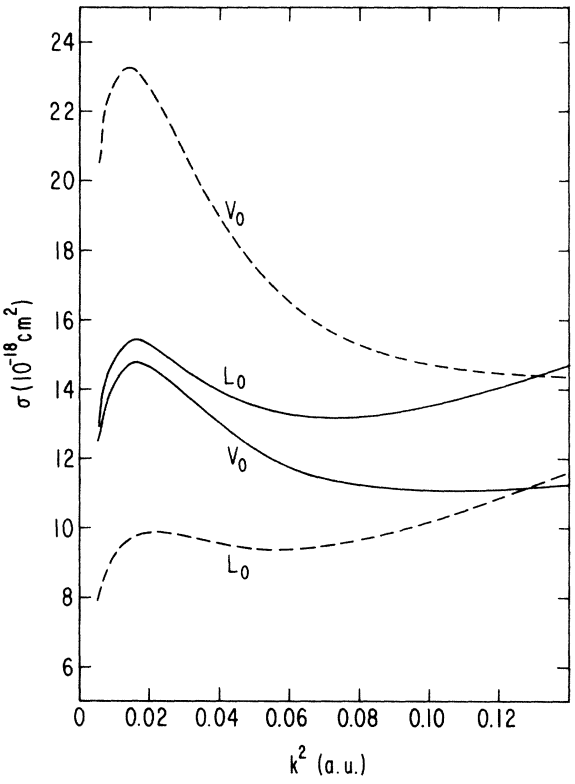

FIG. 9. Cross section of C^- in the single-particle approximation with ϵ_i^{HF} (solid lines) and ϵ_i^{expt} (dotted lines) for the electron affinity. V_0 and L_0 stand for the velocity and length formulas.

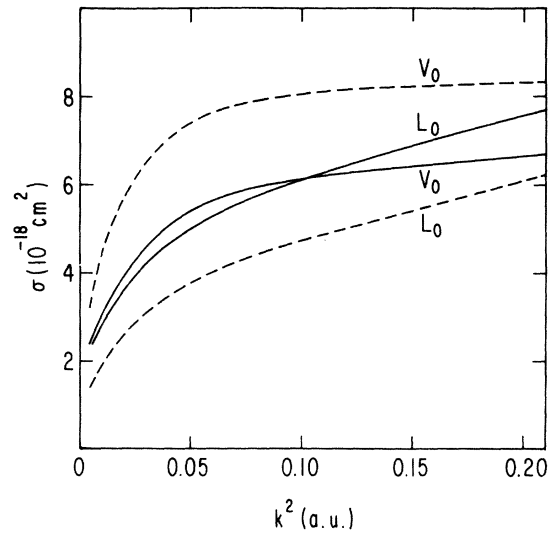

FIG. 10. Cross sections of F^- in the single-particle approximation with ϵ_i^{HF} (solid lines) and ϵ_i^{expt} (dotted lines) for the electron affinity. V_0 and L_0 stand for the velocity and length formulas.

Eq. (7), without changing the wave functions are given diagrammatically by the self-energy insertion to the final-state hole line. Diagram (a) of Fig. 8 is a lowest-order term of this kind. This term has a zero-energy denominator and, in order to get a finite correction, we have to sum up a series of diagrams with various numbers of the same self-energy part in the hole line. This procedure changes ϵ_i^{HF} in Eq. (7) to the value with the second-order correction.

The single-particle-model cross sections, by Eqs. (7) and (9), of C^- and F^- using ϵ_i^{expt} are compared with those using ϵ_i^{HF} in Figs. 9 and 10. We notice the cross sections with ϵ_i^{expt} are far away from the experimental results. The reason for the large length-velocity difference in this case is that the assumption $\epsilon_i = \epsilon_i^{HF}$ for the equivalence of Eqs. (7) and (9) is violated. Without this assumption, Eq. (7) gives a factor $(\epsilon_k - \epsilon_{2p})^2/\omega k$ instead of ω/k in Eq. (9). These facts suggest to us that there must be some other equally important second-order processes which compensate for the correction to the electron affinity. Typical second-order processes, which we have not considered so far, are also shown in Fig. 8. Diagrams (b) and (c) are the effect of the core polarization on the outgoing electron and on the initial-state wave function, respectively. Diagram (d) is the effect of the core rearrangement on the outgoing electron. We feel that the large cancellation in the second-order processes may occur generally for any systems.

The lower-order MBPT calculation based on the Hartree-Fock orbitals may be useful to study the photodetachment processes of negative ions, and it is important in such calculations to use the consistent single-particle energies in the energy-conservation relation.

ACKNOWLEDGMENT

The authors are grateful to Professor Joseph C. Y. Chen for his encouragement throughout the work.

---

*Research supported in part by the U. S. Atomic Energy Commission under Contract AT(04-3)-34PA196, and in part by the National Science Foundation, Grant No. GP 35738X.

[1]T. F. O'Malley, L. Spruch, and L. Rosenberg, J. Math. Phys. 2, 491 (1961); T. F. O'Malley, Phys. Rev. 137, A1668 (1965).

[2]V. P. Myerscough and M. R. C. McDowell, Monthly Notices Roy. Astron. Soc. 128, 287 (1962).

[3]E. J. Robinson and S. Geltman, Phys. Rev. 153, 4 (1967).

[4]H. P. Kelly and A. Ron, Phys. Rev. Lett. 26, 1359 (1971); Phys. Rev. A 5, 168 (1972).

[5]T. Ishihara and R. T. Poe, Phys. Rev. A 6, 116 (1972).

[6]R. L. Chase and H. P. Kelly, Phys. Rev. A 6, 2150 (1972).

[7]T. Ishihara and R. T. Poe, Phys. Rev. A 6, 111 (1972).

[8]H. P. Kelly, Phys. Rev. 136, B896 (1964).

[9]U. Fano and J. W. Cooper, Rev. Mod. Phys. 40, 441 (1968).

[10]E. Clementi, IBM J. Res. Develop. 9, 2 (1965).

[11]See, for example, H. S. Bethe and E. E. Salpeter, *Quantum Mechanics of One and Two Electron Atoms* (Springer-Verlag, Berlin, 1957), Chap. IV.

[12]M. Seman and L. M. Branscomb, Phys. Rev. 125, 1602 (1962).

[13]R. S. Berry and C. W. Reimann, J. Chem. Phys. 38, 1540 (1963).

[14]A. Mandl, Phys. Rev. A 3, 251 (1971).